

1 From complete cross-docking to partners identification and  
2 binding sites predictions

3 Choé Dequeker<sup>1</sup>, Yasser Mohseni Behbahani<sup>1</sup>, Laurent David<sup>1</sup>, Elodie Laine<sup>1,\*</sup> and  
4 Alessandra Carbone<sup>1,2,\*</sup>

5 <sup>1</sup> Sorbonne Université, CNRS, IBPS, Laboratoire de Biologie Computationnelle et Quantitative (LCQB),  
6 75005 Paris, France.

7 <sup>2</sup> Institut Universitaire de France

8 \* corresponding authors: elodie.laine@sorbonne-universite.fr, Alessandra.Carbone@lip6.fr

9 August 22, 2021

## 10 Abstract

11 Proteins ensure their biological functions by interacting with each other. Hence, characterising  
12 protein interactions is fundamental for our understanding of the cellular machinery, and for improving  
13 medicine and bioengineering. Over the past years, a large body of experimental data has been  
14 accumulated on who interacts with whom and in what manner. However, these data are highly  
15 heterogeneous and sometimes contradictory, noisy, and biased. *Ab initio* methods provide a means  
16 to a "blind" protein-protein interaction network reconstruction. Here, we report on a molecular cross-  
17 docking-based approach for the identification of protein partners. We applied it to a few hundred of  
18 proteins, and we systematically investigated the influence of several key ingredients, such as the size  
19 and quality of the interfaces and the scoring function. We achieved some significant improvement  
20 compared to previous works, and a very high discriminative power on some specific functional classes.  
21 In addition, we assessed the ability of the approach to account for protein surface multiple usages,  
22 and we compared it with a sequence-based deep learning method. This work may contribute to  
23 guiding the exploitation of the large amounts of protein structural models now available toward the  
24 discovery of unexpected partners and their complex structure characterisation.

## 25 INTRODUCTION

26 The vast majority of biological processes are ensured and regulated by protein interactions. Hence,  
27 the question of who interacts with whom in the cell and in what manner is of paramount importance  
28 for our understanding of living organisms, drug development and protein design. While proteins con-  
29 stantly encounter each other in the densely packed cellular environment, they are able to selectively  
30 recognise some partners and associate with them to perform specific biological functions. Discrim-  
31 inating between functional and non-functional protein interactions is a very challenging problem.  
32 Many factors may reshape protein-protein interaction networks, such as point mutations, alternative  
33 splicing events and post-translational modifications [1, 2, 3, 4, 5]. Conformational rearrangements  
34 occurring upon binding, and the prevalence of intrinsically disordered regions in interfaces further  
35 increase the complexity of the problem [6, 7, 8, 9]. Ideally, one would like to fully account for this  
36 highly variable setting in an accurate and computationally tractable way.

37 In the past years, a lot of effort has been dedicated to describe the way in which proteins interact  
38 and, in particular, to characterise their interfaces. Depending on the type and function of the  
39 interaction, these may be evolutionary conserved, display peculiar physico-chemical properties or  
40 adopt an archetypal geometry [10, 11, 12, 13, 14, 15, 16, 17, 18, 19, 20]. For example, DNA-binding  
41 sites are systematically enriched in positively charged residues [10] and antigens are recognized by  
42 highly protruding loops [12]. Such properties can be efficiently exploited toward an accurate detection  
43 of protein interfaces [10, 11, 21, 22, 23, 24, 25, 26, 27, 12]. However, the large scale assessment of  
44 predicted interfaces is problematic as our knowledge of protein surface usage by multiple partners is  
45 still very limited [23].

46 A related problem is the prediction of the 3D arrangement formed between two or more protein  
47 partners. This implies generating a set of candidate complex conformations and correctly ranking  
48 them to select those resembling the native structure. Properties reflecting the strength of the asso-  
49 ciation include shape complementarity, electrostatics, desolvation and conformational entropy [28].  
50 Experimental data and evolutionary information (conservation or coevolution signals) may help to  
51 improve the selection of candidate conformations [29, 30, 31]. To address this problem, molecular  
52 docking algorithms have been developed and improved over the past twenty years, stimulated by  
53 the CAPRI competition [32, 33, 34, 35, 36]. Nevertheless, a number of challenges remain, including  
54 the modelling of large conformational rearrangements associated to the binding [37, 32, 38]. More-  
55 over, homology-based modelling often leads to better results than free docking when high-quality  
56 experimental data is available.

57 The development of ultra-fast docking engines exploiting the fast Fourier transform [39, 40, 41],  
58 deep learning [11] and/or coarse-grained protein models [42] has made large-scale docking compu-  
59 tational experiments feasible. Moreover, the availability of 3D structural models from AlphaFold  
60 for entire proteomes [43] has dramatically expanded the applicability of docking algorithms. This  
61 favourable context renders protein-protein interaction network reconstruction accessible at a very  
62 large scale by *ab initio* approaches that avoid biases coming from experimental conditions and allow  
63 for a blind search for partners that may lead to the discovery of new interactions.

64 In a large-scale docking experiment, hundreds or thousands of proteins are either docked to  
65 each other (complete cross-docking, CC-D) or to some arbitrarily chosen proteins. The generated  
66 data can be straightforwardly exploited to predict protein interfaces [44, 23, 45, 46, 47]. Indeed,  
67 randomly chosen proteins tend to dock to localised preferred regions at protein surfaces [48]. In  
68 this respect, the information gathered in the docking experiment can complement sequence- and  
69 structure-based signals detected within monomeric protein surfaces [23]. Beyond interface and 3D

70 structure prediction, very few studies have addressed the question of partner identification. The latter  
71 has traditionally been regarded as beyond the scope of docking approaches. However, an early low-  
72 resolution docking experiment highlighted notable differences between interacting and non-interacting  
73 proteins [49], and we and others [50, 51, 52, 53] have shown that it is possible to discriminate cognate  
74 partners from non-interactors through large-scale CC-D experiments. An important finding of these  
75 studies, already stated in an earlier experiment involving 12 proteins [54], is that relying on the  
76 energy function of the docking algorithm is not sufficient to reach high accuracy. This holds true for  
77 shape complementarity-based energy functions [50], and also for those based on a physical account  
78 of interacting forces [53, 54]. Nevertheless, combining the docking energy with a score reflecting  
79 how well the docked interfaces match experimentally known interfaces allows reaching a very high  
80 discriminative power [53]. Moreover, the knowledge of the global social behaviour of a protein can  
81 help to single out its cognate partner [50, 53]. That is, by accounting for the fact that two proteins  
82 are more or less *sociable*, we can lower down or lift up their interaction strength, and this procedure  
83 tends to unveil the true interacting partners [50]. This notion of sociability also proved useful to  
84 reveal evolutionary constraints exerted on proteins coming from the same functional class, toward  
85 avoiding non-functional interactions [50].

86 In principle, the estimation of systemic properties such as residue binding propensity and protein  
87 sociability shall be more accurate as more proteins are considered in the experiment. But the problem  
88 of discriminating them will also become harder. When dealing with several hundreds of proteins,  
89 the correct identification of the cognate partners requires an incredible accuracy as they represent  
90 only a small fraction of the possible solutions. For instance, a set of 200 proteins for which 100  
91 binary interaction pairs are known will lead to the evaluation of 40 000 possible pairs, and for each  
92 pair several hundreds of thousands candidate conformations (at least) will have to be generated and  
93 ranked.

94 Here, we present a general approach for the identification of protein partners and their discrimi-  
95 nation from non-interactors based on molecular docking. Like our previous efforts [50, 53, 54], this  
96 work aims at handling large ensembles of proteins with very different functional activities and cellular  
97 localisations. Although these classes of proteins appear to have different behaviours, we approach  
98 the problem of partner identification from a global perspective. We report on the analysis of data  
99 generated by CC-D simulations of hundreds of proteins. We combine together physics-based energy,  
100 interface matching and protein sociability, three ingredients we previously showed to be relevant to  
101 partner identification and discrimination. We move forward by investigating what other types of  
102 information may be needed to improve the discrimination. To this end, we systematically explore  
103 the space of parameters contributing to partner identification. These include the scoring function(s)  
104 used to evaluate the docking conformations, the strategy used to predict interacting patches and the  
105 size of the docked interfaces. We show that our approach, CCD2PI (for "CC-D to Partner Identifica-  
106 tion"), reaches a significantly higher discriminative power compared to a previous study addressing  
107 the same problem [53]. We demonstrate that this result holds true overall and also for individual  
108 protein functional classes. Our results emphasise the importance of the docking-inferred residue  
109 binding propensities to drive interface prediction, and the positive contribution of a statistical pair  
110 potential to filter docking conformations. We define a set of default parameter values, with minimal  
111 variations between the different classes, for practical application to any set of proteins. Importantly,  
112 we place ourselves in a context where we do not know the experimental interfaces and use predic-  
113 tions instead. To evaluate CCD2PI predictions, we consider structurally characterised interactions  
114 coming from the Protein Data Bank (PDB) [55] as our gold standard. They are defined based on  
115 docking benchmark annotations [56] or on homology transfer [23]. We show that the protein inter-  
116 action strengths computed by CCD2PI are in good agreement with available structural data. We

117 discuss the implications of these strengths for protein functions. This work paves the way to the au-  
118 tomated *ab initio* reconstruction of protein-protein interaction networks with structural information  
119 at the residue resolution. Since, the reconstruction is based on docking calculations, it is not biased by  
120 specific targets nor by the limitations of experimental techniques.

## 121 RESULTS

### 122 Computational framework

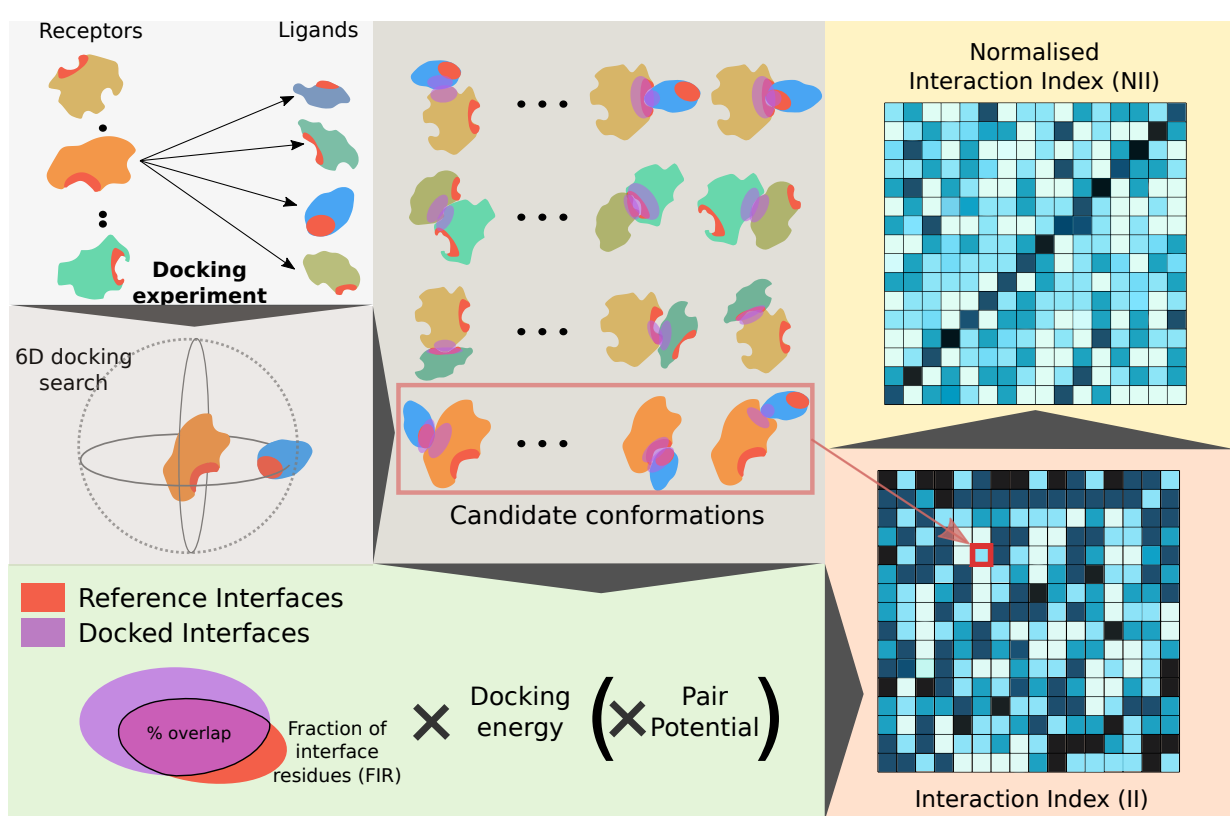


Figure 1: **Principle of the method.** We start from an all-to-all docking experiment (top left panel). Each protein is docked to all proteins in the set. By convention, in each docking calculation, we define a *receptor* and a *ligand*. The red patches on the protein surfaces correspond to predicted interfaces. For a given protein pair  $P_1P_2$ , we generate a pool of conformations associated with energies (top middle panel). Here, both the predicted interfaces and the docked interfaces are highlighted by patches, in red and purple respectively. One can readily see whether they overlap or not. The extent of this overlap (Fraction of Interface Residue) is multiplied by the docking energy to evaluate each docking conformation (bottom left panel). Optionally, we also consider a statistical pair potential in the formula. The best score is computed over all docking conformations and assigned to the protein pair. By doing the same operation for all pairs we compute a matrix of interaction indices (bottom right panel, the darker the higher). If the receptor and the ligand play equivalent roles in the docking calculations, then the matrix will be symmetrical. Otherwise, two different docking calculations are performed for each protein pair  $P_1P_2$  and the matrix will be asymmetrical, as shown here. These indices are then normalised to account for proteins' global social behaviour, hopefully allowing for singling out the cognate partners (top right panel). In the example here, the cognate pairs are ordered on the diagonal.

123 The workflow of CCD2PI is depicted in Figure 1. We exploit data generated by CC-D experiments  
124 performed on hundreds of proteins. In the present work, the CC-D was performed using  
125 the rigid-body docking tool MAXDo [54]. The proteins are represented by a coarse-grained model  
126 and the interactions between pseudo-atoms are evaluated using Lennard-Jones and Coulombic terms  
127 [42]. For each protein pair, MAXDo generated several hundreds of thousands of candidate complex  
128 conformations (Fig. 1, top left panel). Each one of these conformations is evaluated by computing  
129 the product between the overlap between the docked interface (DI) and some reference interface (RI),  
130 a docking energy (either from MAXDo or another one, see *Materials and Methods*), and a statistical  
131 pair potential [57] (optional). The rationale is that a valid conformation should both be energetically  
132 favorable and represents a 3D arrangement compatible with the expected location of the interacting  
133 surfaces. The DIs are detected based on interatomic distances using our efficient algorithm INT-  
134 Builder [58]. The RIs are predicted using sequence- and structure-based properties of single proteins  
135 [12], as well as a systemic property, namely residue binding propensities inferred from the CC-D [23]  
136 (see *Materials and Methods*).

137 Hence, given two proteins  $P_1$  and  $P_2$ , we estimate the interaction index of  $P_1$  with respect to  $P_2$   
138 as

$$II_{P_1, P_2} = \min(FIR_{P_1, P_2} \times E_{P_1, P_2} [\times PP_{P_1, P_2}]), \quad (1)$$

139 where  $FIR_{P_1, P_2}$  (Fraction of Interface Residues) is the fraction of the DIs composed of residues  
140 belonging to the (predicted) RIs for the two proteins,  $E_{P_1, P_2}$  is the docking energy (negative value)  
141 and  $PP_{P_1, P_2}$  is a pair potential score which may or may not be included in the formula. The latter  
142 evaluates the likelihood of the observed residue-residue interactions and might bring complementary  
143 information with respect to the docking energy. We use CIPS [57], a high-throughput software  
144 designed to swiftly reduce the search space of possible native conformations with a high precision.  
145 The minimum is computed over the whole set or a pre-filtered subset of docking conformations (see  
146 *Materials and Methods*). One should note that in the general case,  $II_{P_1, P_2}$  and  $II_{P_2, P_1}$  come from two  
147 different docking runs and are not necessarily equal. This is because the receptor and ligand surfaces  
148 are not explored in an equivalent manner by the docking algorithm (see *Materials and Methods*).

149 The computed interaction indices (Fig. 1, **matrix at the bottom right**) are then normalised  
150 to account for the protein global social behaviour. Formally, the  $II$  values are weighted using the  
151 sociability index (S-index) [50], defined as

$$S_{P_i} := \frac{1}{2|\mathcal{P}|} \sum_{P_j \in \mathcal{P}} II_{P_i, P_j} + II_{P_j, P_i}, \quad (2)$$

152 where  $\mathcal{P}$  is the ensemble of proteins, including  $P_i$ . The normalised interaction index  $NII$  between  
153  $P_1$  and  $P_2$  is computed as a symmetrised ratio of interaction indices (see *Materials and Methods*).  
154 Finally, the  $NII$  values are scaled between 0 and 1 and  $NII_{P_1, P_2} = 1$  when  $P_2$  is the protein predicted  
155 as interacting the most strongly with  $P_1$  (Fig. 1, matrix on the top right).

156 **CCD2PI accurately singles out cognate partners within specific functional  
157 classes**

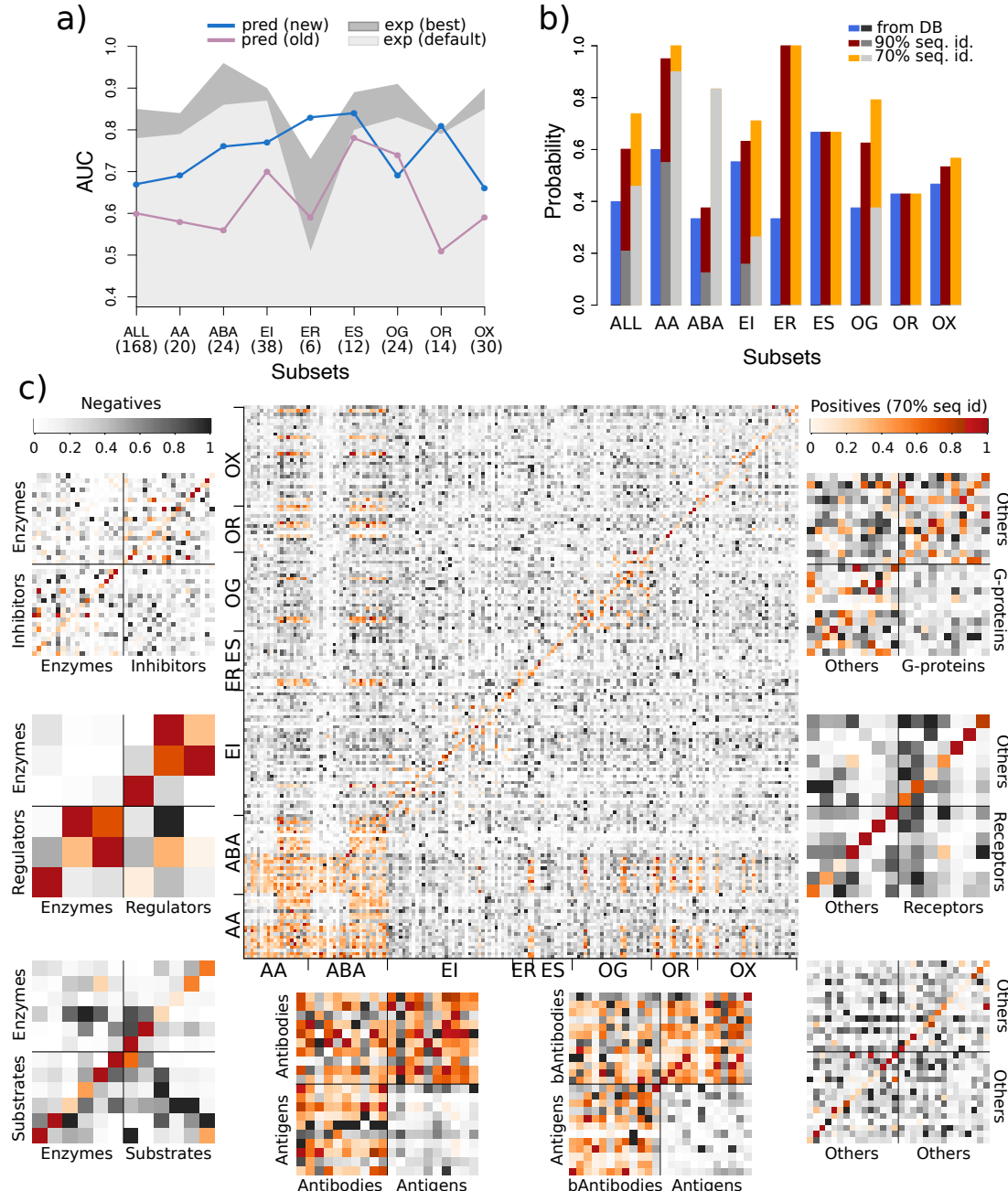


**Figure 2: Predictive performance on the PPDBv2.** (a) AUC values computed for the whole dataset and for the different functional classes. For each protein, we consider one "true" cognate partner, defined from the PPDBv2 annotations. The results obtained with CCD2PI are indicated by the blue curve. For comparison, we also show the results reported in [53] in purple. The areas in grey tones give the discriminative power reached when exploiting the knowledge of the experimental interfaces, using either our default parameters (in light gray) or parameters optimized for such interfaces (in dark gray, see also *Materials and Methods*). The number of proteins in each subset is indicated in parenthesis. (b) Probability of retrieving at least one experimentally known partner in the top 20% of CCD2PI predictions, for each subset. The partners are defined based on the PPDBv2 annotations (in blue) or are inferred from complex PDB structures involving homologs of the proteins from the PPDBv2, at the 90% (in dark red) or 70% (in orange) sequence identity level (see *Materials and Methods*). The bars in grey tones give the probability expected at random. (c) NII matrices computed by CCD2PI. The proteins are ordered on the x-axis such that the *receptors* (e.g. antibodies) appear first, and then the *ligands* (e.g. antigens). They are ordered on the y-axis such that the cognate pairs annotated in PPDBv2 are located on the diagonal. The orange tones highlight the experimentally known interacting pairs (annotated in the PPDBv2 and transferred by homology). AA: antibody-antigen, ABA: bound antibody-antigen. EI: enzyme-inhibitor. ER: enzyme with regulatory or accessory chain. ES: enzyme-substrate. OG: other-with-G-proteins. OR: other-with-receptor. OX: others.

158 We assessed the discriminative power of CCD2PI on a set of 168 proteins forming 84 experimentally  
159 determined binary complexes (Protein-Protein Docking Benchmark v2, PPDBv2, see *Methods*). Here,  
160 we place ourselves in a context where we seek to identify one "true" partner, annotated in the  
161 PPDBv2, for each protein from the benchmark. Over all possible 28 224 interacting pairs, the  
162 cognate partners were singled out with an Area Under the Curve (AUC) of 0.67 (**Fig. 2a**). In the  
163 matrix of predicted NII values (**Fig. 2c**), one can appreciate the relatively small number of pairs  
164 displaying high interaction strengths compared to the enormous number of potential pairs. In this  
165 respect, the contribution of the normalisation stands out as instrumental (**Fig. S1a-b**, compare the  
166 number of dark spots between the *II* and *NII* matrices).

167 We further assessed the ability of CCD2PI to identify the PPDBv2 cognate partners among pro-  
168 teins coming from the same functional class (**Fig. 2a**, blue curve). The partnerships between bound  
169 antibodies and their antigens (*ABA*), between enzymes and their inhibitors, substrates, or regulatory  
170 chains (*EI*, *ES*, *ER*) and between the other proteins and their receptors (*OR*) are particularly well  
171 detected (AUC>0.75). By contrast, the subset regrouping everything that could not be classified  
172 elsewhere (others, *OX*) is the most difficult to deal with. This subset likely contains proteins in-  
173 volved in signalling pathways and establishing transient interactions through modified sites, such  
174 as phosphorylated sites. As a consequence, correctly predicting their interfaces may be particularly  
175 challenging. Conformational changes occurring upon binding seem to play a role as the antibody-  
176 antigen cognate pairs are better detected when the antibodies are bound (**Fig. 2a**, compare *AA* and  
177 *ABA*).

178 The AUC values achieved by CCD2PI are systematically and significantly better than those  
179 computed with our previous pipeline (**Fig. 2a**, compare the blue and purple curves), or similar  
180 in the case of the other-with-G-protein class (*OG*). Replacing the predicted RIs by the interfaces  
181 extracted from the PDB complex structures, which can be seen as *perfect* predictions, leads to  
182 increased AUC values for almost all classes (**Fig. 2a**, areas in grey tones, and **Fig. S1c-d**). This  
183 suggests that proteins competing for the same region at the protein surface do not target exactly the  
184 same set of residues. Knowing exactly which residues are involved in an interaction greatly helps in  
185 the identification of the partner. Of course, this *perfect* knowledge is generally inaccessible in a fully  
186 predictive context. In fact, the predicted interfaces might give a more realistic view on protein surface  
187 usage since they tend to better match *interacting regions* [23], defined from several experimental  
188 structures and representing the interface variability induced by molecular flexibility and multi-partner  
189 binding. Noticeably, the advantage of experimental over predicted RIs reduces or even cancels out  
190 for the small subsets (<15 proteins, *ER*, *ES* and *OR*). This suggests that approximations in the  
191 definition of the interfaces do not influence partner identification when few proteins are considered.

## 192 The interaction strengths predicted by CCD2PI reveal the multiplicity 193 of protein interactions

194 To estimate the agreement between the interaction strengths predicted by CCD2PI and experimental  
195 data, we extended the set of "true" partners by homology transfer. Specifically, we looked in the PDB  
196 for 3D structures of complexes involving homologs of the proteins from PPDBv2 (see *Materials and*  
197 *Methods*). We considered that a structurally characterized interaction found for  $P'_1$  and  $P'_2$ , homologs  
198 of  $P_1$  and  $P_2$ , respectively, was a strong indicator of the possibility for  $P_1$  and  $P_2$  to interact with each  
199 other. Nevertheless, we should stress that homology transfer does not guarantee that the interaction  
200 between  $P_1$  and  $P_2$  is functional in the cell. We identified 585 interacting pairs from homologs  
201 sharing more than 90% sequence identity with the proteins from PPDBv2, and 1 834 at the 70%  
202 sequence identity level (**Fig. 2c**, cells colored in orange). Newly detected interactions are particularly  
203 abundant between antibodies and antigens and among antibodies (**Fig. 2c** and **Fig. S2a-c**). Some

204 of the homology-transferred partners are direct competitors of the cognate partners annotated in  
205 PPDBv2 as they target the same region at the protein surface. Depending on the approximations  
206 in the predicted RI, the former may be more favoured than the latter by CCD2PI. A few examples  
207 of homology-transferred partners better ranked than the PPDBv2-annotated partners are shown in  
208 **Fig. S3**. Overall, the probability of finding at least one "true" partner in the top 20% predictions  
209 is almost systematically increased when extending the set of positives (**Fig. 2b**). For instance,  
210 71% (27 out of 38) of the proteins from the *EI* subset have at least one partner inferred at more  
211 than 70% sequence identity ranked in the top 7. Moreover, the homology-transferred interactions  
212 tend to populate the regions of the matrices displaying high interaction strengths (**Fig. 2c** and  
213 **Fig. S2d**). For instance, CCD2PI predictions suggest that antigens tend to avoid each other much  
214 more than antibodies, and indeed much more homology-transferred interactions are found among  
215 antibodies, compared to antigens (*AA* and *ABA*). A similar trend is also observed for the enzyme-  
216 regulator (*ER*) and enzyme-substrate (*ES*) and other-with-G-protein (*OG*) subsets (**Fig. 2c** and  
217 **Fig. S2d**). We observe more predicted and experimental regulator-regulator and substrate-substrate  
218 interactions than enzyme-enzyme interactions, and more other-other interactions than interactions  
219 among G proteins.

## 220 The ingredients of partner discrimination

221 CCD2PI comprises four main hyper-parameters potentially influencing the results (**Table I**),  
222 namely (a) the distance threshold used to detect the DI, (b) the scoring strategy used to pre-  
223 dict the RI, (c) the docking energy function used to compute *II*, and (d) the optional inclusion of  
224 the pair potential in the *II* formula. The distance threshold modulates the size of the DI while  
225 the scoring strategy influences how close the RI are from the experimentally known interfaces. The  
226 choice of the energy function and that of using or not the pair potential directly impact the cal-  
227 culation of the interaction index. In order to avoid the risk of overfitting, we strove to determine  
228 global default parameter values (**Table I**, see also *Materials and Methods*). In the following, we  
229 report on a systematic analysis of the influence of the parameters on the discriminative power of the  
230 approach, also by considering functional classes (**Fig. 3**). The total number of possible parameter  
231 combinations is 72, and we focused on the top 15, for the whole dataset and for its eight subsets.  
232 Given a parameter under study, the pool of 15 top combinations was divided by the set of possible  
233 values for the parameter (see *Materials and Methods*).

234 Table I: Main hyper-parameters of CCD2PI

Docked interfaces Distance threshold (in Å)	Predicted interfaces Scoring strategy	Docking energy <sup>a</sup> (E)	Pair potential <sup>b</sup> (PP)
4.5	SC-mix	<b>MAXDo</b>	<b>CIPS</b>
<b>5</b>	SC-monoSeed-mix	iATTRACT	None
6	<b>SC-dockSeed-mix</b> SC-juxt	PISA	

235 The default parameter values are highlighted in bold. They were optimized on PPDBv2 (see *Methods*). <sup>a</sup>  
236 MAXDo was chosen for all functional classes but EI and ER, where it was replaced by PISA and  
iATTRACT respectively. <sup>b</sup> CIPS was used for all functional classes but OR.

234 The estimation of the match between the DI and the RI depends on the way the former are  
235 detected and on the strategy adopted to predict the latter. We observed that varying the distance  
236 threshold used to detect the DI between 4.5 and 6 Å does not significantly impact the discrimi-

237 nation on the whole dataset, nor on most of the functional classes (**Fig. 3a**). Nevertheless, it is  
238 clearly preferable to define smaller than bigger DIs for the identification of antibody-antigen cognate  
239 pairs (**Fig. 3a**, see *AA* and *ABA*). Interestingly, this trend is not observed when using experimen-  
240 tal interfaces as RIs (**Fig. 5b**). This suggests that as the DIs grow, residues not specific to the  
241 cognate interactions but present in the predicted RIs are being considered. To predict interfaces,  
242 we considered four main strategies, each one of them comprising between 3 and 4 scoring schemes  
243 (**Fig. S4** and see *Materials and Methods*). Our algorithm relies on four descriptors, evolutionary  
244 conservation, physico-chemical properties, local geometry and docking-inferred binding propensities,  
245 and the strategies differ in the way we combine these properties. The one leading to the best results  
246 on the whole dataset and also on a couple of functional classes is SC-dockSeed-mix (**Fig. 3b**, see  
247 *ABA* and *OX*). In this scoring scheme, the *seed* of the predicted interface is defined based on the  
248 propensities of protein surface residues to be targeted in the docking calculations. Then, the seed is  
249 extended combining these docking propensities with evolutionary, geometrical and physico-chemical  
250 properties (see *Materials and Methods*). The strategy leading to the worst results, SC-monoSeed-mix,  
251 introduces the docking propensities only after seed detection. The seeds are detected because they  
252 are highly conserved or protruding. SC-monoSeed-mix is not even found in the top 15 combinations  
253 of parameters for the whole dataset, nor for the enzyme-substrate and *other* classes (**Fig. 3b**). This  
254 emphasises the crucial role of the docking propensities to drive the interface predictions.

255 Regarding the docking energy, we considered MAXDo, iATTRACT and PISA. MAXDo and  
256 iATTRACT are very similar as they include the same contributions (see *Materials and Methods*).  
257 They mainly differ in the treatment of the clashes, better tolerated in iATTRACT, and of the  
258 electrostatic contribution, more persistent at long distances in iATTRACT. PISA is different as it  
259 estimates the likelihood of a macromolecular assembly to be functionally relevant based on chemical  
260 thermodynamics (see *Materials and Methods*). While all three energies perform almost equally well  
261 on the whole dataset, with a little advantage for MAXDo, the results on the individual subsets are  
262 more contrasted (**Fig. 3c**). In particular, PISA is the only energy function appearing in the top 15  
263 combinations for the enzyme-inhibitor subset (*EI*) while MAXDo is the only one for the other-with-  
264 G-protein subset (*OG*). Finally, we investigated the influence of including or not the statistical pair  
265 potential CIPS to compute the interaction index (**Fig. 3d**). While CIPS improves the discrimination  
266 for the antibody-antigen subsets (*AA* and *ABA*), it is clearly detrimental for the other-with-receptor  
267 class (*OR*). The extent of these impacts may vary depending on the energy function with which  
268 CIPS is paired, but the trends are consistent from one energy function to another. The picture is  
269 very different when we replace the predicted RIs by experimental interfaces (**Fig. S5d**). In this  
270 context, CIPS is mostly contributing in a negative way to the identification of the cognate partners.  
271 This suggests that CIPS may underrate some near-native conformations. Although this would not  
272 affect much the results when the RIs are predicted, since the number of incorrect conformations  
273 removed largely surpasses the number of near-native conformations wrongly removed, this could  
274 prove detrimental when using the experimental interfaces, especially in a context where the number  
275 of positives is very small compared to that of negatives.

## 276 **Small approximations in the reference interfaces may significantly impact 277 partner identification**

278 We further characterised the relationship between the ability of singling out cognate partners and  
279 the resemblance between the predicted and the experimental interfaces. The average F1-values of  
280 the predicted interfaces range between 0.37 and 0.58 (**Fig. 3e**). The strategy leading to the best  
281 AUC values for partner discrimination, namely SC-dockSeed-mix, gives the most accurate predicted  
282 interfaces overall (**Fig. 3e-g, ALL**). It is also significantly more precise than the other strategies

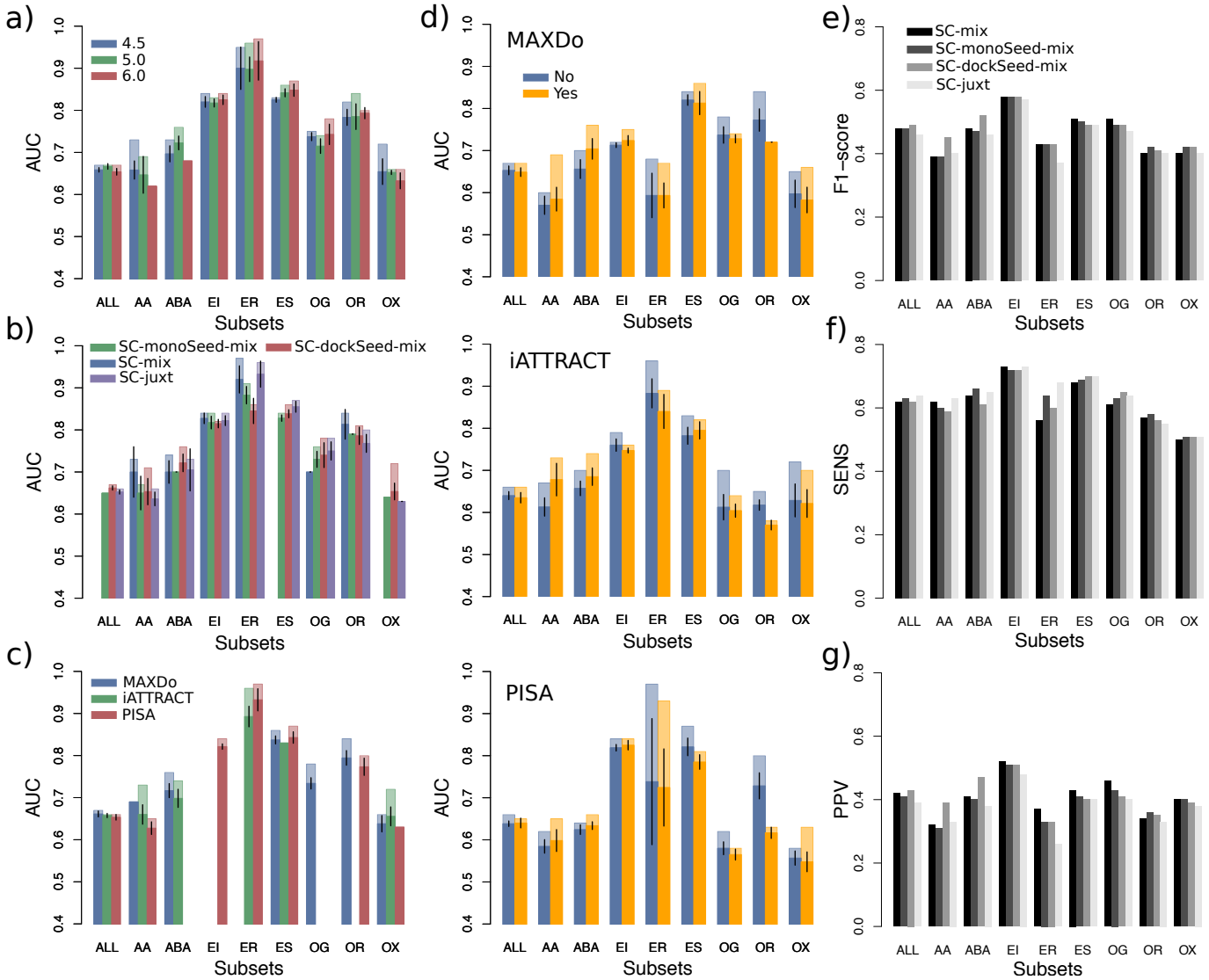


**Figure 3: Influence of the parameters for PPDBv2.** (a-d) Variation of the AUC values upon parameter changes. The four parameters considered are: (a) the distance threshold used to define docked interfaces, (b) the scoring strategy used to predict interfaces, (c) the docking energy, and (d) the presence or absence of the pair potential, depending on the docking energy. In each plot, for each protein class, we considered the 15 combinations yielding the highest AUC values, among all 72 possible combinations. For a given parameter, the different bars correspond to a partition of this combination set according to the possible values of the parameter. If a parameter value was not present in the 15 best combinations, then it does not appear on the plot. We report the average AUC values (in opaque) and the maximum AUC values (in transparent). The black segments indicate the intervals  $[\mu - 2\sigma_\mu, \mu + 2\sigma_\mu]$ , where  $\mu$  is the mean and  $\sigma_\mu$  is the standard error of the mean. (e-g) Resemblance between predicted and experimental interfaces. (e) F1-score. (f) Sensitivity. (g) Positive predictive value.

in the detection of the antibody-antigen interfaces (Fig. 3e-g, AA and ABA). Looking across the different classes, it is *a priori* not obvious to assess a direct correlation between the quality of the predicted interfaces and the discriminative power of the approach. In particular, the three subsets (ER, ES and OR) for which predicted RIs lead to AUCs as good as those obtained with experimental RIs (Fig. 2a) do not stand out for the quality of their predicted interfaces (Fig. 3e-g).

288 g). This confirms that when dealing with few proteins (<15), working with approximate interfaces  
289 do not hamper the identification of the cognate partners. However, if we disregard these subsets,  
290 then we find that the ability to detect the cognate pairs is highly correlated with the F1-score and the  
291 precision of the predicted interfaces (Fig. S6). The Pearson correlation coefficient is of 0.86 (resp.  
292 0.90) between the AUC values and the F1-scores (resp. positive predictive values, PPV) computed  
293 for SC-dockSeed-mix.

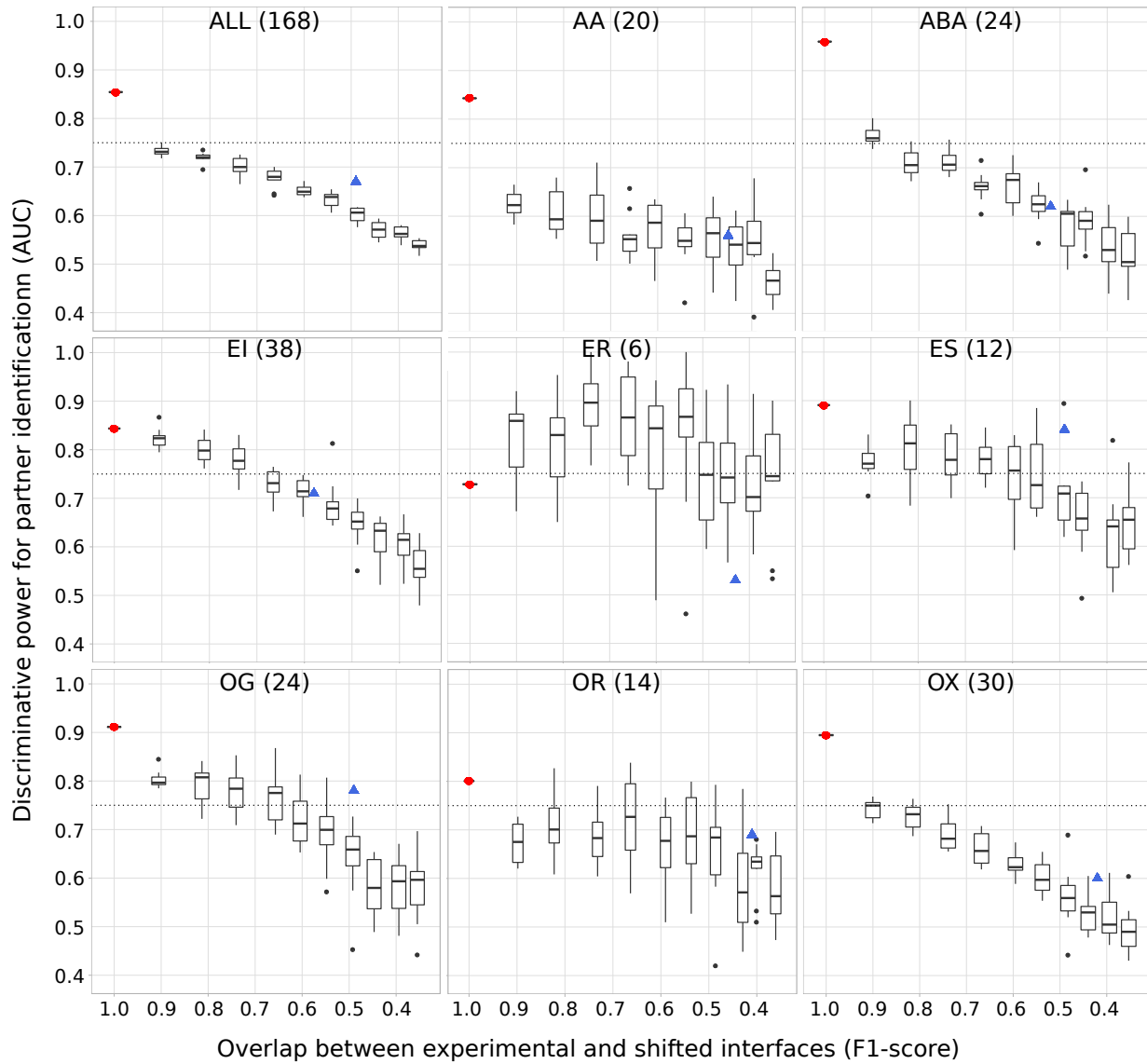


Figure 4: **Sensitivity of partner identification to approximations in the reference interfaces.** The RIs were obtained by gradually shifting the experimental interfaces (see *Materials and Methods*). On each plot, we show 10 boxes corresponding to 10 different shift magnitudes. Each box comprises 10 AUC values obtained from 10 random generations of shifts in interfaces at a given amplitude. The values in x-axis give the average F1-scores computed for these shifted interfaces. The red dot and the blue triangle indicate the performance achieved using the experimental interfaces and the interfaces predicted by SC-dockSeed-mix as RIs, respectively. To compute the AUCs, we used the parameters identified as the best ones when using the experimental interfaces as RIs, namely a distance threshold of 6Å, the MAXDo docking energy, and without CIPS.

294 To investigate more precisely the sensitivity of partner discrimination with respect to approxi-

mations in the RIs, we generated shifted decoys from the experimental interfaces. For each interface in the dataset, we moved between 10 and 100% of its residues, by increments of 10% (see *Materials and Methods*). This allowed us to control the deviation of our RIs with respect to the experimentally known interfaces of the cognate interactions. We observed that the AUC computed for partner identification decreases as the shifted decoys share less and less residues in common with the experimental interfaces (**Fig. 4**). The only notable exception is the smallest class, namely *ER*, which displays a chaotic behaviour. The two other smallest classes, *ES* and *OR* also show some chaotic variations, to a lesser extent. On the whole dataset, the AUC drops by 0.12 when the interfaces are shifted by 10%, corresponding to an F1-score of 0.9. A similar or even bigger gap is observed for all subsets comprising more than 15 proteins, except the enzyme-inhibitor subset (*EI*). On the whole dataset, the two antibody-antigen subsets (*AA* and *ABA*) and the *other* subset (*OX*), we identify cognate partners with an AUC lower than 75% with shifted decoys that still match very well (F1-score >0.8) the experimental interfaces. This shows that many competing proteins are able to bind favourably to almost the same protein surface region as the cognate partner. Compared to the shifted interfaces, our predicted interfaces allow reaching a similar or better partner discrimination for all classes but *ER*.

### 311 Accounting for protein surface multiple usage

312 Next, we assessed CCD2PI on an independent set of 62 proteins for which we defined some *interacting regions* accounting for the multiple usage of a protein surface by several partners and for 313 molecular flexibility [23]. More precisely, we obtained each *interacting region* by merging overlapping 314 interacting sites detected in the biological assemblies (from the PDB) involving the protein itself 315 or a close homolog (with >90% sequence identity, see *Materials and Methods*). These regions can 316 be seen as binding "platforms" for potentially very different partners. In this experiment, we used 317 predicted interfaces as RIs, and all of them match well the experimentally known interacting regions 318 (F1-score>0.6). CCD2PI identifies at least one known partner in the top 3 for about a third of the 319 proteins (**Fig. 5a**, inset). For instance, the Bcl-2-like protein 11 (2nl9:B), known partner of the Mcl-1 320 protein (2nl9:A), is ranked second (**Fig. 5a**). The top predicted partner for Mcl-1, a tropomyosin 321 construct (2z5h:B), shares the same  $\alpha$ -helical shape. For trypsin-3 (2r9p:A), six proteins are pre- 322 dicted as better binders as its known inhibitor (2r9p:E). An extreme example is given by the heme 323 oxygenase, whose interaction with itself is very poorly ranked (**Fig. 5a**). This may be explained by 324 the fact that the homodimer is asymmetrical, with two different interaction sites for the two copies, 325 one of them not being taken into account by CCD2PI.

### 327 Comparison with a sequence-based deep learning approach

328 Finally, we compared CCD2PI with DPPI [59], a deep learning method predicting protein interactions 329 from sequence information only. DPPI takes as input two query proteins, each represented by 330 a sequence profile, and outputs a score reflecting the probability that they physically interact. The 331 parameters of the architecture are learnt from experimentally known interactions. We re-trained the 332 architecture to assess its performance on PPDBv2 (see *Materials and Methods*). DPPI is able to 333 single out the known partners (annotated in the database or inferred at >90% identity) with a very 334 high accuracy, reaching an AUC of 95% versus 79% for CCD2PI. Yet, for a subset of 20 proteins, we 335 obtained better ranks for the known partners (**Fig. 5b**). These proteins belong to different functional 336 classes. Two of them, namely 1i4d\_r and 1he1\_r (according to the PPDBv2 nomenclature) are copies 337 of the human Rac GTPase (Uniprot id: P63000). In total, Rac GTPase appears in three complexes 338 from PPDBv2, 1i4d, 1he1 and 1e96, where it interacts with its three known partners. While the

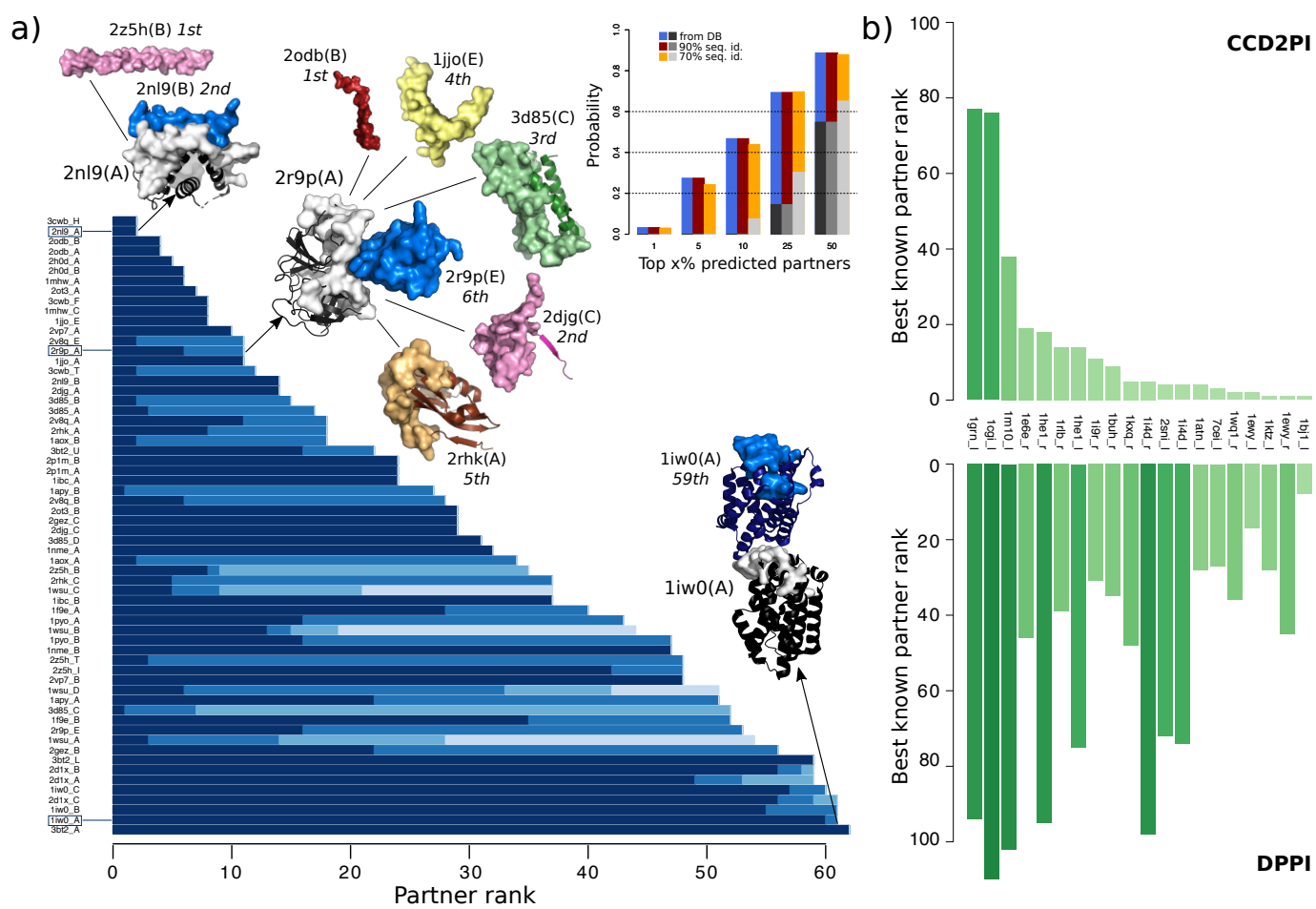


Figure 5: **Assessment of CCD2PI on an independent dataset, and comparison with a sequence-based deep learning method.** (a) Partner discrimination on an independent set of 62 proteins where RIs can accommodate different partners. The main barplot gives the rank(s) determined by CCD2PI for the known partner(s) of each protein and its close homologs (>90% sequence identity). Each blue tone correspond to a known partner within the set. The 3D structures of three proteins from the set are depicted as black cartoons with their RIs highlighted in grey surface. Their known partners are shown in colors and their interacting regions are depicted as surfaces. For the complex between two copies of 1iw0:A, the position and orientation of the copies was taken from the PDB structure 1wzg. The barplot in inset gives the probability of retrieving at least one known partner in the top x% predicted partners. (b) Comparison with DPPI. Best known partner ranks obtained from CCD2PI (on top) and DPPI (at the bottom). We focus on the subset of proteins for which the ranks provided by CC2PI are better.

339 three partners are identified in the top 5 by DPPI when using 1e96.l as the query, they are ranked  
 340 between 95 and 101 when using 1i4d\_r or 1he1\_r. The three query sequences display near-perfect  
 341 sequence identities, but they cover more or less extended portions of the protein. Hence, the discrep-  
 342 ance between the results reveals a substantial sensitivity of DPPI with respect to different sequence  
 343 contexts. The lack of a detection may be explained by an altered balance between signal and noise  
 344 or between different signals coming from different interactions, or by some missing out-of-interface  
 345 signal relevant for the interaction. In that case, we observed that our docking-based approach is  
 346 more robust, as it finds at least one partner in the top 18 whatever the query.

## 347 DISCUSSION

348 We have proposed a general approach to identify protein partners from large-scale docking ex-  
349 periments. We found that cognate partners can be singled out with high accuracy within specific  
350 functional classes. Beyond this parameter, we have identified a number of factors contributing to  
351 improving the discriminative power of the approach. We have primarily placed ourselves in a con-  
352 text where we seek to identify only one "true" partner for a given protein, while the other studied  
353 proteins are considered as non-interactors. We have found that in such conditions, the definition of  
354 the binding interface should be very precise to allow achieving high discriminative power. In reality,  
355 most proteins interact with multiple partners, via overlapping or distinct regions at their surface.  
356 Our current knowledge and understanding of the multiplicity of protein surface usage is still very lim-  
357 ited. To move forward, we have collected experimentally characterised protein complexes among the  
358 proteins in our benchmark set and also among their close homologs. The rationale was that protein  
359 interactions tend to be conserved among close homologs, as evidenced by the success of homology-  
360 based prediction of protein complex 3D structures. This analysis revealed many possible interactions  
361 between the studied proteins, and showed that these interactions tend to populate regions in our  
362 predicted matrices displaying high interaction strengths. Hence, the propensities of interaction in-  
363 ferred from docking agree with the available structural data. As more complexes will be structurally  
364 characterised, we expect that the "experimental" interaction matrix will resemble more and more the  
365 predicted one, *i.e.* with many dark spots (high values). A limitation of both experimental structural  
366 data and our computational framework is that they often cannot determine whether a protein-protein  
367 interaction will be functional or not in the cell. For instance, many antibody-antigen interactions  
368 can be inferred by homology transfer while the specificity of such interactions is very high and de-  
369 termined by only a few residues. A previous cross-docking study also highlighted the importance of  
370 the backbone conformation of the antibody to obtain a high-quality docked interface and thus be  
371 able to discriminate binders from non-binders [60]. More generally, the role of short peptide motifs  
372 for substrate selectivity and protein specific functions is being widely recognised [61], and there are  
373 documented examples of enzymes sharing high sequence identity while targeting different substrates  
374 [62]. Sequence-based learning approaches may overcome these limitations, but they do not provide  
375 direct information about the role of each residue in the formation and/or stabilisation of the assembly  
376 yet. From this perspective, sequence-based motif or specificity-determining site detection approaches  
377 could help to guide the docking toward boosting the accuracy of complex configuration prediction  
378 and to improve functional annotations of protein interactions. Such a combination of approaches  
379 may be particularly useful to distinguish multiple (potentially overlapping) interfaces.

## 380 MATERIALS AND METHODS

### 381 Protein datasets

382 The first dataset is the Protein-Protein Docking Benchmark 2.0 (PPDBv2) [56] (<https://zlab.umassmed.edu/benchmark/>), which comprises 168 proteins forming 84 binary complexes. Each pro-  
383 tein may be comprised of one or several chains, and is designated as receptor (r) or ligand (l). For  
384 most of the proteins, we used the unbound crystallographic structures for the docking calculations.  
385 The 12 notable exceptions are antibodies for which the unbound structure is unavailable and the  
386 bound structure was used instead. As there are also unbound antibodies present in the dataset,  
387 we can evaluate the impact of conformational changes on the results. The complexes of PPDBv2  
388 are grouped in eight classes (Fig. S1a) following [63]: antibody-antigen (AA, 20 proteins), bound  
389 antibody-antigen (ABA, 24), enzyme-inhibitor (EI, 38), enzyme with regulatory or accessory chain

391 (ER, 6), enzyme-substrate (ES, 12), other-with-G-protein (OG, 24), other-with-receptor (OR, 14)  
392 and others (OX, 30). Note that for three cases, namely 1IR9, 1KXQ and 2HMI, there was an inversion  
393 in the original dataset between receptor and ligand, which we fixed here.

394 The second dataset is the P-262 benchmark introduced in [23]. It comprises 262 single protein  
395 chains for which single and multiple partners interactions are known in the PDB. We used bound  
396 conformations found in complex structures for the docking calculations. This dataset was extracted  
397 from a larger set of 2246 protein chains defined in the scope of the HCMD2 project (see <http://www.ihes.fr/~carbone/HCMDproject.htm>). Based on the information recovered from the PDB,  
398 the proteins were manually classified in eleven groups (Fig. S1b), following and extending the  
399 classification proposed [63]. Hence, the set is comprised of 16 bound antibodies (AB), 25 complex  
400 subunits (C), 60 enzymes (E), 10 enzyme regulators (ER), 9 G proteins (G), 6 antigens from the  
401 immune system (I), 23 receptors (R), 24 structural proteins (S), 16 substrates/inhibitors (SI), 7  
402 transcription factors (TF) and 66 proteins with other function (O).

## 404 Interacting pair identification by homology transfer

405 We extended the set of known partners by transferring knowledge from close homologs. Specifically,  
406 we exploited the pre-computed PDB homology clusters with 90% and 70% sequence identities. For  
407 each protein pair considered, we verified the existence of a physical contact between the proteins in  
408 the pair, or some homologs at 90% (resp. 70%) sequence identity. Two proteins were considered to  
409 be in a contact if their interface was larger than 5 residues, as detected by INTBuilder [58]. This  
410 procedure was performed at the protein chain level. To deal with the multi-chain proteins from  
411 PPDBv2, we considered that two proteins were in interaction whenever at least one pair of chains  
412 from the two proteins was in interaction.

## 413 Cross-docking calculations

414 Given an ensemble of proteins, complete cross-docking consists in docking each protein against all the  
415 proteins in the dataset, including itself. All calculations were performed by the MAXDo (Molecular  
416 Association via Cross Docking) algorithm [54].

## 417 Reduced protein representation

418 The protein is represented using a coarse-grain protein model [42] where each amino acid is repre-  
419 sented by one pseudoatom located at the C $\alpha$  position and either one or two pseudoatoms representing  
420 the side-chain (with the exception of Gly). Interactions between the pseudoatoms are treated using a  
421 soft Lennard Jones (LJ) type potential with parameters adjusted for each type of side-chain (see Ta-  
422 ble 1 in [42]). In the case of charged side-chains, electrostatic interactions between net point charges  
423 located on the second side-chain pseudoatom were calculated by using a distance-dependent dielectric  
424 constant  $\epsilon = 15r$ , leading to the following equation for the interaction energy of the pseudoatom pair  
425  $i, j$  at distance  $r_{ij}$ :

$$E_{ij} = \left( \frac{B_{ij}}{r_{ij}^8} - \frac{C_{ij}}{r_{ij}^6} \right) + \frac{q_i q_j}{15r_{ij}^2} \quad (3)$$

426 where  $B_{ij}$  and  $C_{ij}$  are the repulsive and attractive LJ-type parameters respectively, and  $q_i$  and  $q_j$  are  
427 the charges of the pseudoatoms  $i$  and  $j$ . More details about the representation can be found in [54].

## 428 Systematic docking simulations

429 MAXDo implements a multiple energy minimization scheme similar to that of ATTRACT [42] where  
430 proteins are considered as rigid bodies. For each protein pair, one protein (called the receptor) is is  
431 fixed in space, while the second (called the ligand) is placed at multiple positions on the surface  
432 of the receptor. For each pair of receptor/ligand starting positions, different starting orientations  
433 are generated by applying rotations of the gamma Euler angle defined with the axis connecting the  
434 centers of mass of the 2 proteins. We used two different protocols to explore the docking space for  
435 our two datasets. In the case of PPDBv2, the whole surface of the receptor was probed by the  
436 ligand. This was guaranteed by generating starting positions that covered the whole surface and  
437 restraining the ligand motions during the simulation so as to maintain its center of mass on a vector  
438 passing through the center of mass of the receptor protein. As a result, the receptor and the ligand  
439 are treated differently and given en protein pair  $P_1P_2$ , docking  $P_1$  against  $P_2$  is not equivalent to  
440 docking  $P_2$  against  $P_1$ . More details about this protocol can be found in [54, 53]. In the case of  
441 P-262, the ensemble of starting positions was restricted using predictions from the JET method [13].  
442 This reduced the docking search space by up to 50%. Moreover, the restrain was removed, so that  
443 the ligand was free to migrate to a position completely different from its starting position. Thus,  
444 for each couple of proteins  $P_1P_2$ , considering  $P_1$  as the receptor and  $P_2$  as the ligand is essentially  
445 equivalent to the reverse situation where  $P_2$  is the receptor and  $P_1$  is the ligand. More details about  
446 this protocol can be found in [64].

## 447 Computational implementation

448 For each pair, several hundreds of thousands of energy minimizations were performed. As each  
449 minimization takes 5 to 15 s on a single 2 GHz processor, a CC-D of several hundreds of proteins would  
450 require several thousand years of computation. However, the minimizations are independent from  
451 each other and thus can be efficiently parallelized on grid-computing systems. Our calculations have  
452 been carried out using the public World Community Grid (WCG, [www.worldcommunitygrid.org](http://www.worldcommunitygrid.org)),  
453 with the help of thousands of internauts donating their computer time to the project. It took  
454 approximately seven months to perform CC-D calculations on the PPDBv2, and three years on the  
455 complete HCMD2 dataset (2246 proteins) from which P-262 is extracted. More technical details  
456 regarding the execution of the program on WCG can be found in [65]. The data analysis was partly  
457 realized on Grid'5000 (<https://www.grid5000.fr>).

## 458 Data Analysis

### 459 Detection and prediction of interface residues

460 The docked interfaces are defined by the sets of residues from the two partners closer than  $d$  Å.  
461 They were computed using INTBuilder [58], and we considered three values for  $d$ , 4.5, 5 and 6. The  
462 experimental interfaces were detected in the X-ray structures of the cognate complexes using the  
463 same tool and a distance  $d$  of 5 Å.

464 The reference interfaces were predicted using a modified version of dynJET<sup>2</sup> [23], a software tool  
465 predicting interacting patches based on four residue descriptors. Specifically, dynJET<sup>2</sup> relies on three  
466 sequence- and structure-based properties of single proteins, *i.e.* evolutionary conservation, physico-  
467 chemical properties and local geometry (measured by the circular variance), and on a systemic  
468 property reflecting docking-inferred binding propensities (Fig S4, see also [23] for more detailed  
469 definitions). dynJET<sup>2</sup> algorithm first detects the *seed* of the patch, then *extends* it and finally add  
470 an *outer layer* [12]. At each step, surface residues are selected using a combination of the four  
471 descriptors. Four scoring strategies are implemented, to cover a wide range of interfaces. The first

472 one,  $SC_{cons}$  detects highly conserved residues and then grows the patches with residues less and  
473 less conserved and more and more protruding, and likely to be found at interfaces based on their  
474 physico-chemical properties. The second one,  $SC_{notLig}$  is a variant of  $SC_{cons}$  where local geometry is  
475 accounted for in the seed detection step to avoid buried ligand-binding pockets. The third one,  $SC_{geom}$   
476 disregards evolutionary conservation and looks for protruding residues with good physico-chemical  
477 properties. The fourth one,  $SC_{dock}$ , defines patches exclusively comprised of residues frequently  
478 targeted in docking calculations. We refer to this group of  $SC$ s as  $SC$ -*juxt*. We modified dynJET<sup>2</sup> to  
479 create 9 additional scoring schemes grouped in 3 main strategies, namely  $SC$ -*mix*,  $SC$ -*monoSeed*-*mix*  
480 and  $SC$ -*dockSeed*-*mix* (**Fig S4**). All 9 scoring schemes are variants of  $SC_{cons}$ ,  $SC_{notLig}$  and  $SC_{geom}$   
481 including the docking-inferred binding propensities in different ways.  $SC$ -*mix* combines them with  
482 the other descriptors at each step.  $SC$ -*monoSeed*-*mix* detects the seeds using only the single-protein  
483 based properties, and then combines the latter with the docking propensities to grow the patches.  
484  $SC$ -*dockSeed*-*mix* relies exclusively on the docking propensities to detect the seeds and then grows  
485 them using a combination of all four descriptors. We implemented all scoring schemes in dynJET<sup>2</sup>.  
486 For each protein, given a chosen main strategy, we detected a set of predicted patches using all its  
487 scoring schemes. Each patch was defined as a consensus of at least 2 iterations over 10 of dynJET<sup>2</sup>.  
488 We then retained the patch or combination of patches matching the best the experimentally known  
489 interfaces.

490 We also used shifted decoys as reference interfaces. To generate them, we gradually shifted the  
491 experimentally known interfaces from the PPDBv2. For each experimental interface, we randomly  
492 generated 100 decoys, by moving between 10% and 100% of its residues. More precisely, the first 10  
493 decoys were generated by moving 10% of the residues, the next 10 by moving 20%, etc... At each  
494 step of the algorithm, we randomly pick up an interface residue  $r_s$  located at the border, *i.e.* at less  
495 than 5 Å of a surface residue that is not part of the interface. Then, we identify the interface residue  
496 located the farthest away from  $r_s$ , and we randomly pick up one of its neighbours  $r_n$  (< 5 Å). We  
497 then switch the status of  $r_s$  and  $r_n$ . In other words,  $r_s$  is removed from the interface and  $r_n$  is added  
498 to the interface. The residue  $r_s$  cannot be picked again in the following iteration.

#### 499 Re-scoring of the docking models

500 We considered three scoring functions, namely iATTRACT [66], PISA [67] and CIPS [57], in replace-  
501 ment or complement of the one implemented in MAXDo.

502 iATTRACT [66] is a docking software more recent than MAXDo and mixing a rigid-body docking  
503 approach with flexibility. The energy function is similar to that of MAXDo, except that the repulsive  
504 term in the Lennard-Jones potential decreases more rapidly with the interatomic distance while the  
505 electrostatic contribution decreases less rapidly. Specifically, iATTRACT interaction energy of the  
506 pseudoatom pair  $i, j$  at distance  $r_{ij}$  is expressed as

$$E_{ij} = \left(\frac{\sigma_{ij}}{r_{ij}}\right)^{12} - \left(\frac{\sigma_{ij}}{r_{ij}}\right)^6 + \frac{q_i q_j}{\epsilon r_{ij}} \quad (4)$$

507 where  $\sigma_{ij}$  is the LJ-type parameter,  $q_i$  and  $q_j$  are the charges of the pseudoatoms  $i$  and  $j$ , and the  
508 dielectric constant  $\epsilon$  is set to 10. Each of the docking models obtained from the CC-D was subjected  
509 to iATTRACT's minimisation process and we used the energy value coming from this minimization.

510 PISA [67] is a scoring method developed to discriminate between biological and non biological  
511 complexes. It relies on the dissociation free energy to evaluate the stability of a complex. On top of  
512 the dissociation free energy, PISA considers larger assemblies more probable than the smaller ones  
513 and considers that single-assembly sets take preference over multi-assembly sets. We used PISA to  
514 re-score the docking conformations produced by MAXDo.

515 CIPS [57] is a statistical pair potential meant to be used as a high throughput technique able to  
516 largely filter out most of the non-native conformations with a low error rate. It was trained using  
517 230 bound structures from the Protein-Protein Docking Benchmark 5.0 [68]. We used it to obtain  
518 complementary scores on the docking conformations.

519 **The protein Interaction Index - II**

520 We evaluate docking models using an interaction index  $II$  computed as a product between three  
521 terms (see Eq. 1). For a given protein pair  $P_1P_2$ , the first term,  $FIR_{P_1,P_2}$ , is the overall fraction of  
522 the docked interfaces composed of residues belonging to the reference interfaces for the two proteins:  
523  $FIR_{P_1,P_2} = FIR_{P_1} * FIR_{P_2}$ . It reflects the agreement between the docked interfaces and the reference  
524 interfaces. The reference interfaces may be experimentally known or predicted. The second one,  
525  $E_{P_1,P_2}$ , is the docking energy provided by MAXDo, PISA or iATTRACT. The third one,  $PP_{P_1,P_2}$  is  
526 the value computed by CIPS and it may or may not be included in the formula. The product is  
527 computed for every docking conformations and the minimum (best) value is kept.

528 **The protein Normalized Interaction Index - NII**

529 To account for the global social behavior of the proteins, we further normalize the interaction indices.  
530 The normalized interaction index  $NII$  between  $P_1$  and  $P_2$  was determined as

$$NII_{P_1,P_2} = \frac{\min(II'_{P_1,P_2}, II'_{P_2,P_1})^4}{\min_P(II'_{P_1,P}) \cdot \min_P(II'_{P,P_2}) \cdot \min_P(II'_{P,P_1}) \cdot \min_P(II'_{P_2,P})} \quad (5)$$

531 where  $II'_{P_1,P_2}$  is a symmetrized weighted version of the interaction index  $II_{P_1,P_2}$  and it is defined as:

$$II'_{P_1,P_2} := \frac{II_{P_1,P_2}}{\sqrt{S_{P_1} \cdot S_{P_2}}}, S_{P_i} := \frac{1}{2|\mathcal{P}|} \sum_{P_j \in \mathcal{P}} II_{P_i,P_j} + II_{P_j,P_i} \quad (6)$$

532 where  $\mathcal{P}$  is the ensemble of proteins considered. The normalization can be applied to the whole  
533 dataset or to subsets. In either case,  $NII$  values vary between 0 and 1. For each protein  $P_i$ , we  
534 defined its predicted partner as the protein  $P_j$  leading to  $NII_{P_i,P_j} = 1$ .

535 **Parameter setting**

536 The four main parameters of our approach and the different values we considered are reported in Table  
537 I. They were optimized on the PPDBv2. For each subset, we computed 72 AUC values corresponding  
538 to the 72 possible combinations of parameter values. Then, we ranked the combinations based on  
539 their weighted average AUC values. Given a combination  $C_i$ , the average was computed as

$$\overline{AUC}(C_i) = \frac{\sum_{j=1}^n (N_j \times AUC^j(C_i))}{\sum_{j=1}^n N_j}, \quad (7)$$

540 where  $N_j$  is the number of proteins in the subset  $j$  and  $n$  is the number of subsets. We considered as  
541 subsets the eight functional classes and also the entire dataset itself, leading to  $n = 9$ . The weighting  
542 minimises the effect a subset with a low number of proteins could have on the global ranking, while  
543 putting more importance on subsets with a large number of proteins. The combination maximizing  
544 the value of  $\overline{AUC}(C_i)$  was chosen as the default one (**Table I**, in bold).

545 Then, for each class  $j$ , we ranked the 72 possible combinations according to their AUC values,  
546  $AUC^j(C_i)$ , and we retained the top 20%, hence 15 combinations. This pool was separated by each

547 one of the four parameters. Whenever we found a parameter value leading to a better AUC than  
548 the default value, we further assessed this difference with a Mann Whitney U-test [69, 70]. For this  
549 test, we went back to the whole ensemble of 72 combinations and compared the distributions of AUC  
550 values obtained with the default value and the other value, respectively. If the p-value was lower  
551 0.01, then we considered the other value to significantly improve our discrimination potency over the  
552 default one. And we decided to use it for the given class.

553 We applied the same procedure when dealing with the experimental interfaces. Since the num-  
554 ber of possible combinations (18) is much lower in that case, we retained the top 30%, hence 6  
555 combinations.

## 556 Comparison with DPPI

557 We re-trained DPPI architecture [59] on the Profppikernel database [71] containing 44 000 interactions  
558 (10% positive). The positive samples were taken from the HIPPIE database [72]. We removed from  
559 the training set all sequences which share more than 70% identity with any sequence from PPDBv2.  
560 We clustered the samples such that any two sequences do not share more than 40% identity. We  
561 used MMseqs2 [73] to cluster and filter sequences.

562 **Acknowledgements** The MAPPING project (ANR-11-BINF-0003, Excellence Programme “In-  
563 vestissement d’Avenir”); funds from the Institut Universitaire de France; the access to the HPC  
564 resources of the Institute for Scientific Computing and Simulation (Equip@Meso project - ANR-10-  
565 EQPX- 29-01, Excellence Program “Investissement d’Avenir”); the World Community Grid (WCG,  
566 [www.worldcommunitygrid.org](http://www.worldcommunitygrid.org)) and WCG volunteers that allowed us to perform cross-docking ex-  
567 periments with MAXDo on the PPDBv2.0.

568 **Competing interests** The authors declare no competing interests.

## 569 References

570 [1] Weako J, Gursoy A, Keskin O. Mutational effects on protein–protein interactions. *Protein*  
571 *Interactions: Computational Methods, Analysis And Applications*. 2020;p. 109.

572 [2] Yang X, Coulombe-Huntington J, Kang S, Sheynkman GM, Hao T, Richardson A, et al. Widespread expansion of protein interaction capabilities by alternative splicing. *Cell*.  
573 2016;164(4):805–817.

575 [3] Bowler EH, Wang Z, Ewing RM. How do oncoprotein mutations rewire protein–protein interaction  
576 networks? *Expert review of proteomics*. 2015;12(5):449–455.

577 [4] Grossmann A, Benlasfer N, Birth P, Hegele A, Wachsmuth F, Apelt L, et al. Phospho-tyrosine  
578 dependent protein–protein interaction network. *Molecular systems biology*. 2015;11(3).

579 [5] Woodsmith J, Stelzl U. Studying post-translational modifications with protein interaction net-  
580 works. *Current opinion in structural biology*. 2014;24:34–44.

581 [6] Zanzoni A, Ribeiro DM, Brun C. Understanding protein multifunctionality: from short linear  
582 motifs to cellular functions. *Cellular and Molecular Life Sciences*. 2019;p. 1–6.

583 [7] Mosca R, Pache RA, Aloy P. The role of structural disorder in the rewiring of protein interactions  
584 through evolution. *Molecular & Cellular Proteomics*. 2012;11(7).

585 [8] Zacharias M. Accounting for conformational changes during protein–protein docking. *Current*  
586 *opinion in structural biology*. 2010;20(2):180–186.

587 [9] Bonvin AM. Flexible protein–protein docking. *Current opinion in structural biology*.  
588 2006;16(2):194–200.

589 [10] Corsi F, Lavery R, Laine E, Carbone A. Multiple protein-DNA interfaces unravelled by evolution-  
590 ary information, physico-chemical and geometrical properties. *PLOS Computational Biology*.  
591 2020;16(2):e1007624.

592 [11] Gainza P, Sverrisson F, Monti F, Rodola E, Boscaini D, Bronstein M, et al. Deciphering in-  
593 teraction fingerprints from protein molecular surfaces using geometric deep learning. *Nature*  
594 *Methods*. 2020;17(2):184–192.

595 [12] Laine E, Carbone A. The geometry of protein-protein interfaces reveals the multiple origins of  
596 recognition patches. *PLoS Computational Biology*. 2015;11(12):e1004580.

597 [13] Engelen S, Trojan LA, Sacquin-Mora S, Lavery R, Carbone A. Joint evolutionary trees: a large-  
598 scale method to predict protein interfaces based on sequence sampling. *PLoS Comput Biol*.  
599 2009;5(1):e1000267.

600 [14] Chakrabarti P, Janin J. Dissecting protein-protein recognition sites. *Proteins*. 2002  
601 May;47(3):334–343.

602 [15] Glaser F, Steinberg DM, Vakser IA, Ben-Tal N. Residue frequencies and pairing preferences at  
603 protein-protein interfaces. *Proteins*. 2001 May;43(2):89–102.

604 [16] Jones S, Marin A, Thornton JM. Protein domain interfaces: characterization and comparison  
605 with oligomeric protein interfaces. *Protein Eng*. 2000 Feb;13(2):77–82.

606 [17] Bogan AA, Thorn KS. Anatomy of hot spots in protein interfaces. *J Mol Biol.* 1998 Jul;280(1):1–9.

607

608 [18] Larsen TA, Olson AJ, Goodsell DS. Morphology of protein-protein interfaces. *Structure.* 1998 Apr;6(4):421–427.

609

610 [19] Tsai CJ, Lin SL, Wolfson HJ, Nussinov R. Studies of protein-protein interfaces: a statistical analysis of the hydrophobic effect. *Protein Sci.* 1997 Jan;6(1):53–64.

611

612 [20] Lichtarge O, Bourne HR, Cohen FE. An evolutionary trace method defines binding surfaces common to protein families. *J Mol Biol.* 1996;257(2):342–358.

613

614 [21] Zeng M, Zhang F, Wu FX, Li Y, Wang J, Li M. Protein–protein interaction site prediction through combining local and global features with deep neural networks. *Bioinformatics.* 2020;36(4):1114–1120.

615

616

617 [22] Zhang J, Kurgan L. SCRIBER: accurate and partner type-specific prediction of protein-binding residues from proteins sequences. *Bioinformatics.* 2019;35(14):i343–i353.

618

619 [23] Dequeker C, Laine E, Carbone A. Decrypting protein surfaces by combining evolution, geometry, and molecular docking. *Proteins: Structure, Function, and Bioinformatics.* 2019;87(11):952–965.

620

621 [24] Zhang J, Kurgan L. Review and comparative assessment of sequence-based predictors of protein-binding residues. *Briefings in bioinformatics.* 2018;19(5):821–837.

622

623 [25] Ripoche H, Laine E, Ceres N, Carbone A. JET2 Viewer: a database of predicted multiple, possibly overlapping, protein-protein interaction sites for PDB structures. *Nucleic Acids Res.* 2017 Apr;45(7):4278.

624

625

626 [26] Esmaielbeiki R, Krawczyk K, Knapp B, Nebel JC, Deane CM. Progress and challenges in predicting protein interfaces. *Briefings Bioinf.* 2016 Jan;17(1):117–131.

627

628 [27] Aumentado-Armstrong TT, Istrate B, Murgita RA. Algorithmic approaches to protein-protein interaction site prediction. *Algorithms Mol Biol.* 2015;10:7.

629

630 [28] Gabb HA, Jackson RM, Sternberg MJ. Modelling protein docking using shape complementarity, electrostatics and biochemical information. *Journal of molecular biology.* 1997;272(1):106–120.

631

632 [29] Quignot C, Rey J, Yu J, Tufféry P, Guerois R, Andreani J. InterEvDock2: an expanded server for protein docking using evolutionary and biological information from homology models and multimeric inputs. *Nucleic acids research.* 2018;46(W1):W408–W416.

633

634

635 [30] Van Zundert G, Rodrigues J, Trellet M, Schmitz C, Kastritis P, Karaca E, et al. The HADDOCK2. 2 web server: user-friendly integrative modeling of biomolecular complexes. *Journal of molecular biology.* 2016;428(4):720–725.

636

637

638 [31] Hopf TA, Schärfe CP, Rodrigues JP, Green AG, Kohlbacher O, Sander C, et al. Sequence co-evolution gives 3D contacts and structures of protein complexes. *Elife.* 2014;3:e03430.

639

640 [32] Lensink MF, Brysbaert G, Nadzirin N, Velankar S, Chaleil RA, Gerguri T, et al. Blind prediction of homo-and hetero-protein complexes: The CASP13-CAPRI experiment. *Proteins: Structure, Function, and Bioinformatics.* 2019;87(12):1200–1221.

641

642

643 [33] Lensink MF, Wodak SJ. Blind predictions of protein interfaces by docking calculations in  
644 CAPRI. *Proteins*. 2010;78(15):3085–3095.

645 [34] Janin J, Henrick K, Moult J, Eyck LT, Sternberg MJ, Vajda S, et al. CAPRI: a Critical  
646 Assessment of PRdicted Interactions. *Proteins*. 2003;52(1):2–9.

647 [35] Smith GR, Sternberg MJ. Prediction of protein–protein interactions by docking methods. *Current  
648 opinion in structural biology*. 2002;12(1):28–35.

649 [36] Wodak SJ, Janin J. Computer analysis of protein-protein interaction. *Journal of molecular  
650 biology*. 1978;124(2):323–342.

651 [37] Vakser IA. Challenges in protein docking. *Current Opinion in Structural Biology*. 2020;64:160–  
652 165.

653 [38] Lensink MF, Velankar S, Kryshtafovych A, Huang SY, Schneidman-Duhovny D, Sali A, et al.  
654 Prediction of homoprotein and heteroprotein complexes by protein docking and template-based  
655 modeling: A CASP-CAPRI experiment. *Proteins: Structure, Function, and Bioinformatics*.  
656 2016;84:323–348.

657 [39] Ohue M, Shimoda T, Suzuki S, Matsuzaki Y, Ishida T, Akiyama Y. MEGADOCK 4.0: an ultra–  
658 high-performance protein–protein docking software for heterogeneous supercomputers. *Bioinfor-  
659 matics*. 2014;30(22):3281–3283.

660 [40] Pierce BG, Hourai Y, Weng Z. Accelerating protein docking in ZDOCK using an advanced 3D  
661 convolution library. *PloS one*. 2011;6(9).

662 [41] Ritchie DW, Venkatraman V. Ultra-fast FFT protein docking on graphics processors. *Bioinfor-  
663 matics*. 2010;26(19):2398–2405.

664 [42] Zacharias M. Protein-protein docking with a reduced protein model accounting for side-chain  
665 flexibility. *Protein Sci*. 2003 Jun;12(6):1271–1282.

666 [43] Tunyasuvunakool K, Adler J, Wu Z, Green T, Zielinski M, Žídek A, et al. Highly accurate  
667 protein structure prediction for the human proteome. *Nature*. 2021;p. 1–9.

668 [44] Schweke H, Mucchielli MH, Sacquin-Mora S, Bei W, Lopes A. Protein interaction energy land-  
669 scapes are shaped by functional and also non-functional partners. *Journal of Molecular Biology*.  
670 2020;.

671 [45] Reille S, Garnier M, Robert X, Gouet P, Martin J, Launay G. Identification and visualization  
672 of protein binding regions with the ArDock server. *Nucleic acids research*. 2018;46(W1):W417–  
673 W422.

674 [46] Vamparys L, Laurent B, Carbone A, Sacquin-Mora S. Great interactions: How binding incorrect  
675 partners can teach us about protein recognition and function. *Proteins*. 2016 Oct;84(10):1408–  
676 1421.

677 [47] Martin J, Lavery R. Arbitrary protein- protein docking targets biologically relevant interfaces.  
678 *BMC biophysics*. 2012;5(1):7.

679 [48] Fernandez-Recio J, Totrov M, Abagyan R. Identification of Protein-Protein Interaction Sites  
680 From Docking Energy Landscapes. *J Mol Biol*. 2004 Jan;335(3):843–865.

681 [49] Vakser IA. Low-resolution docking: Prediction of complexes for underdetermined structures.  
682 *Biopolymers*. 1996;39(3):455–464.

683 [50] Laine E, Carbone A. Protein social behavior makes a stronger signal for partner identification  
684 than surface geometry. *Proteins*. 2017 Jan;85(1):137–154.

685 [51] Maheshwari S, Brylinski M. Across-proteome modeling of dimer structures for the bottom-up  
686 assembly of protein-protein interaction networks. *BMC bioinformatics*. 2017;18(1):257.

687 [52] Ohue M, Matsuzaki Y, Shimoda T, Ishida T, Akiyama Y. Highly precise protein-protein inter-  
688 action prediction based on consensus between template-based and de novo docking methods. In:  
689 *BMC proceedings*. vol. 7. BioMed Central; 2013. p. S6.

690 [53] Lopes A, Sacquin-Mora S, Dimitrova V, Laine E, Ponty Y, Carbone A. Protein-protein inter-  
691 actions in a crowded environment: an analysis via cross-docking simulations and evolutionary  
692 information. *PLoS computational biology*. 2013;9(12).

693 [54] Sacquin-Mora S, Carbone A, Lavery R. Identification of protein interaction partners and protein-  
694 protein interaction sites. *J Mol Biol*. 2008;382:1276–1289.

695 [55] Berman HM, Battistuz T, Bhat TN, Bluhm WF, Bourne PE, Burkhardt K, et al. The Protein  
696 Data Bank. *Acta Crystallogr D Biol Crystallogr*. 2002 Jun;58(Pt 6 No 1):899–907.

697 [56] Mintseris J, Wiehe K, Pierce B, Anderson R, Chen R, Janin J, et al. Protein-Protein Docking  
698 Benchmark 2.0: an update. *Proteins*. 2005;60:214–216.

699 [57] Nadalin F, Carbone A. Protein–protein interaction specificity is captured by contact preferences  
700 and interface composition. *Bioinformatics*. 2018;34(3):459–468.

701 [58] Dequeker C, Laine E, Carbone A. INTerface Builder: A Fast Protein-Protein Interface Recon-  
702 struction Tool. *J Chem Inf Model*. 2017;57(11):2613–2617.

703 [59] Haschemifar S, Neyshabur B, Khan AA, Xu J. Predicting protein–protein interactions through  
704 sequence-based deep learning. *Bioinformatics*. 2018;34(17):i802–i810.

705 [60] Kilambi KP, Gray JJ. Structure-based cross-docking analysis of antibody–antigen interactions.  
706 *Scientific reports*. 2017;7(1):1–15.

707 [61] Lyon KF, Cai X, Young RJ, Mamun AA, Rajasekaran S, Schiller MR. Minimotif Miner 4: a  
708 million peptide minimotifs and counting. *Nucleic acids research*. 2018;46(D1):D465–D470.

709 [62] Barrett K, Lange L. Peptide-based functional annotation of carbohydrate-active enzymes by  
710 conserved unique peptide patterns (CUPP). *Biotechnology for biofuels*. 2019;12(1):102.

711 [63] Brian G, Panagiotis L, Paul A, Alexandre M, et al. Updates to the Integrated Protein–Protein  
712 Interaction Benchmarks: Docking Benchmark Version 5 and Affinity Benchmark Version 2.  
713 *Journal of Molecular Biology*. 2015;.

714 [64] Lagarde N, Carbone A, Sacquin-Mora S. Hidden partners: Using cross-docking calculations to  
715 predict binding sites for proteins with multiple interactions. *Proteins: Structure, Function, and*  
716 *Bioinformatics*. 2018;86(7):723–737.

717 [65] Bertis V, Bolze R, Desprez F, Reed K. From dedicated grid to volunteer grid: large scale  
718 execution of a bioinformatics application. *Journal of Grid Computing*. 2009;7(4):463–478.

719 [66] Schindler CE, de Vries SJ, Zacharias M. iATTRACT: Simultaneous global and local inter-  
720 face optimization for protein–protein docking refinement. *Proteins: Structure, Function, and*  
721 *Bioinformatics*. 2015;83(2):248–258.

722 [67] Krissinel E, Henrick K. Inference of macromolecular assemblies from crystalline state. *Journal*  
723 *of molecular biology*. 2007;372(3):774–797.

724 [68] Vreven T, Moal IH, Vangone A, Pierce BG, Kastritis PL, Torchala M, et al. Updates to the  
725 integrated protein–protein interaction benchmarks: docking benchmark version 5 and affinity  
726 benchmark version 2. *Journal of molecular biology*. 2015;427(19):3031–3041.

727 [69] Bauer DF. Constructing confidence sets using rank statistics. *Journal of the American Statistical*  
728 *Association*. 1972;67(339):687–690.

729 [70] Hollander M, Wolfe DA, Chicken E. *Nonparametric statistical methods*. vol. 751. John Wiley  
730 & Sons; 2013.

731 [71] Hamp T, Rost B. Evolutionary profiles improve protein–protein interaction prediction from  
732 sequence. *Bioinformatics*. 2015;31(12):1945–1950.

733 [72] Schaefer MH, Fontaine JF, Vinayagam A, Porras P, Wanker EE, Andrade-Navarro MA. HIP-  
734 PIE: Integrating protein interaction networks with experiment based quality scores. *PloS one*.  
735 2012;7(2):e31826.

736 [73] Steinegger M, Söding J. MMseqs2 enables sensitive protein sequence searching for the analysis  
737 of massive data sets. *Nature biotechnology*. 2017;35(11):1026–1028.